Design of a Compact Balanced Tri-band Bandpass Filter Using Simple Planar Resonator with Wide Stop-band and High Selectivity

P. Faghir Mirnezami[1], M. Tavakoli[1*], F. Sotoudeh[1], A. Horri[1], R. Eskandari[1]

[1] Department of Electrical Engineering, Arak Branch, Islamic Azad University, Arak, Iran.

ABSTRACT: The most balanced multiband band-pass-filters have some remarkable properties while provide a trade-off between design goals. Additionally, few of them have provided a structure capable of satisfactory harmonic suppression. Stepped Impedance Resonators (SIR) are famous and widely utilized to relocate or cancel high order harmonics, and they provide advantages when used in designing bandpass filters. They have shown benefits in achieving Common Mode (CM) suppression along with compact size and wide stopband. To design a tri-band balanced bandpass filter, a Ring-SIR structure is used as the main building block of the filter. The SIR is first analyzed and the design formulas are presented and the design graphs are extracted based on that. Using the graphs, it is possible to design a tri-band filter and have the ability to control the center frequencies of the pass-bands. To achieve high pass-band selectivity, coupled feeding configuration is chosen external quality factor is analyzed, and respective graphs are presented. Results show more than 20dB isol,ation with pass-bands centering at 1.7, 2.55, and 4.48 GHz, insertion losses of 1.44, 1.77, and 2.11 dB respectively. The corresponding FBWs are 3.95%, 4.10% and 1.56% respectively. Great out-of-band performance is achieved with a wide stop-band stretching from 4.8 to 8.76 GHz. The CM rejection for three pass-bands are better than 12.9, 18.9 and 43.5dB, respectively.

1- Introduction

Different microwave filters have been broadly implemented in microwave wireless communication circuits, such as mobile voice and data services, video, messaging, satellite and long-range radio communications [1]. Among various methods, microstrip filters have extensive implementation in wireless communications and have attracted researchers' interest due to their superiorities such as reduced size, inexpensiveness and simple fabrication [2].

Due to their benefits, such as elevated resilience to electromagnetic interferences, crosstalk and environmental noise and balanced microwave circuits have become very popular in current wireless communication circuits. In multi-purpose communication devices, multi-band differential band pass filters have an important function. Various techniques have been presented for designing multi-band filters. Designing based on the classical filter design theory is used in [3] [4], designing by creating transmission zeros into the transfer function of a wide-band filter is used in [5], Multi-band filters with dual-mode resonators with perturbation are used in [6], Multi-band filters with stepped-impedance multi-mode resonators are used in [7] [8], Multi-band filters with stub-loaded resonators are used in [9], Superposition of stepped-impedance and stub-loaded resonators is used in [10], designing by cascading independent single-band or dual-band filters is an-

other method used in [11].

Few pieces of research have been conducted on the subject of balanced multiband bandpass filters and quasi-elliptic-type technique using multi-stubs was used in [12]. A band-pass-filter with differential-input has been implemented using 5 SLRs with two half-wave-length open stub Transmission Lines (TLs) at the input and output ports of the altered configuration, which could create an additional transmission zero between two bands [13]. The Square-Ring-Loaded-Resonator (SRLR) is a fairly facile method which is appropriate for multi-band filter design. The process of designing a tri-band differential band-pass-filter with high common-mode rejection and extended stop-band using a Square-Ring-Resonator (SRR) approach was proposed in [14]. In [15], researchers have proposed a new balanced tri-band and quad-band microstrip band-pass-filter having adjustable bandwidth based on slot-line coupling method. In differential-mode, the multi-band response was achieved using three and four half-wave-length Transmission Lines for tri-pass and quad pass-band setups, which were used for specific resonance frequencies. Moreover, to further control the resonance response, coupling-coefficient and external quality factors have been adjusted, and as a result, the bandwidth for every pass-band was also controlled. Design based on octo-section SIRR has been proposed in [16].

*Corresponding author's email: m-tavakoli@iau-arak.ac.ir.
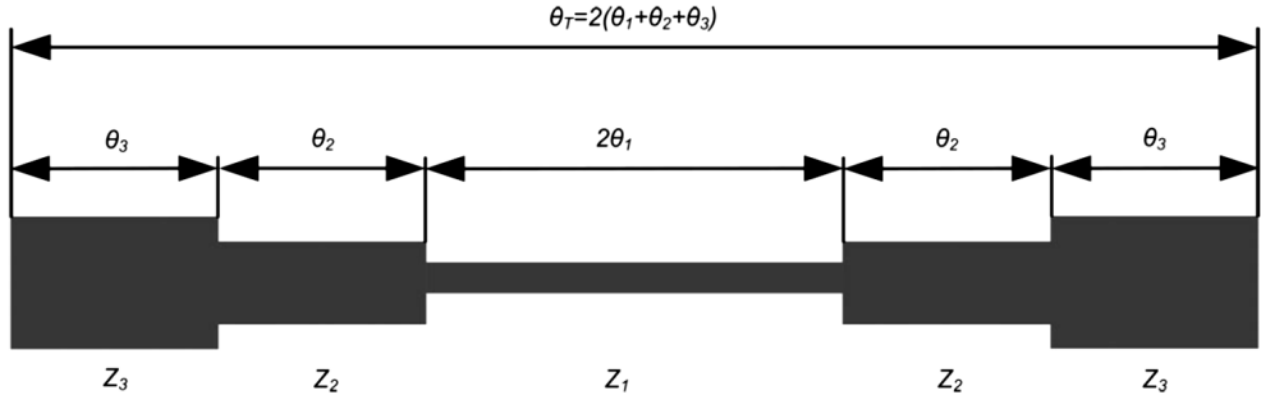
Fig. 1. Configuration of tri-stage stepped-impedance resonator.

Additionally, a balanced quad-band microstrip band-pass-filter that has controllable frequency response and 3-dB fractional bandwidth based on the slot-line approach is designed in [17]. BPFs composed of conventional microstrip line resonators usually suffer from high conductor loss. To overcome this problem, [18] has used High-Temperature Superconducting (HTS) materials to design a balanced tri-band superconducting band-pass filter, which has to be kept below transition temperature (usually -196.15° Celsius), involving expensive cryogenic technology.

While most balanced multiband band-pass-filters have some remarkable properties, they provide a trade-off between DM performance, CM suppression, size, complicated techniques and controllability.

Among different methods, SIRs are famous and widely utilized to relocate or cancel high order harmonics. Researches have also shown that they provide advantages when used in designing bandpass filters [19].

This article proposes a simple configuration using SIR for designing a balanced tri-band BPF. The most significant features of the proposed structure are its ultra-wide upper DM stopband, high CM rejection in pass-bands, tunability of pass-bands, high suppression in DM stopbands, low insertion loss and highly selective response. Moreover, in contrast to circuits using complicated techniques and expensive fabrication process (such as lumped elements, Via, DGS and HTS), the resonator implemented in this filter is simple and easy to fabricate.

In SIRs, multiple modes do not stem from coupled degenerative modes, but they are formed by the fundamental and higher-order mode where thr resonance frequencies are not harmonically related as in conventional structures [20].

The novelty of the presented balanced BPF is that by using non-conventional multi-mode SIR resonator structure, remarkable frequency response in differential-mode is realized. Compared to conventional SIRs with only two parameters (impedance ratio of steps), this paper uses a more complicated design process which involves five design parameters, giving the designer more degrees of freedom in controlling the response of the circuit.

In order to investigate its behavior, the presented tri-band balanced bandpass filter is studied, full-wave simulation is performed, and measurements are made on fabricated prototype. The proposed analytical method used in this study consists of using common-mode and differential mode circuit analysis, delivering equations relation as a means of confirmation. Ultimately, the measurements are made using the network analyzer. Results show valid agreement between the mathematical analysis and measured results. Hence, to verify the design theory, a prototype tri-band band-pass-filter operating at frequencies of 1.7/2.55/ 4.48 GHz for Advanced Wireless Services (AWS), LTE, and long-distance radio telecommunication applications is developed, respectively.

2- Analysis of SIR Structure and its Properties

The tri-mode stepped-impedance resonator can be realized (i.e., a structure that supports three resonance modes). Fig. 1 shows a stepped-impedance resonator having three segments with different impedances.

The synthesis technique of conventional SIR-based filters relies on the condition of $\theta_1=\theta_2=\theta_3$. Under these circumstances, the analytical method could be applied; if $\theta_1 \neq \theta_2 \neq \theta_3$, a novel synthesis approach should be used as basic analytical techniques do not suffice. The approach mentioned above consists of numerical approximation analysis that has a fairly simple implementation despite the number of existing parameters.

Even-mode and odd-mode analysis could be applied to investigate the performance of the circuit. The equivalent circuits are presented in Fig. 2 and the expressions for input impedances are given in the following form:

$$(1)$$
$$Z_{ino} = j\frac{Z_1Z_2Z_3\tan\theta_1+Z_2^2Z_3\tan\theta_2+Z_2Z_3^2\tan\theta_3-Z_1Z_3^2\tan\theta_1\tan\theta_2\tan\theta_3}{Z_2Z_3-Z_1Z_3\tan\theta_1\tan\theta_2-Z_1Z_2\tan\theta_1\tan\theta_3-Z_2^2\tan\theta_2\tan\theta_3}$$

$$(2)$$
$$Z_{ine} = j\frac{Z_2^2Z_3\tan\theta_1\tan\theta_2+Z_2Z_3^2\tan\theta_1\tan\theta_3+Z_1Z_3^2\tan\theta_2\tan\theta_3-Z_1Z_2Z_3}{Z_2Z_3\tan\theta_1+Z_1Z_3\tan\theta_2+Z_1Z_2\tan\theta_3-Z_2^2\tan\theta_1\tan\theta_2\tan\theta_3}$$
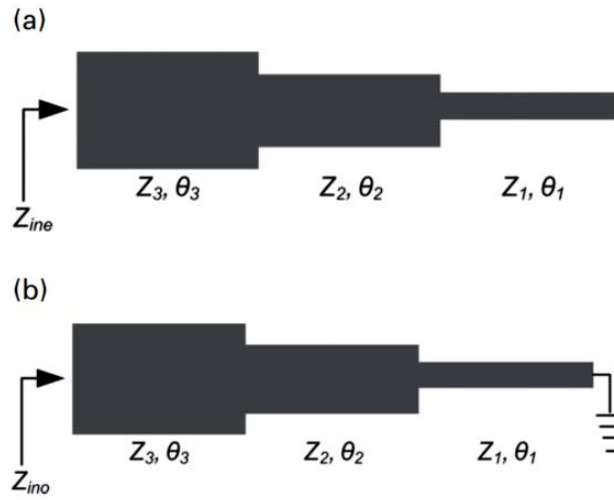
Fig. 2. Equivalent circuit for: (a) Even- (b) Odd-Mode.

Where Z_1, Z_2 and Z_3 are the characteristic impedances and θ_1, θ_2 and θ_3 are their electrical lengths.

Considering K_1 to be the ratio of Z_2/Z_1 and K_2 the ratio of Z_3/Z_2, and considering the resonance condition of $Y_{ino}=1/Z_{ino}=0$, the differential mode resonance frequencies could be calculated as:

$$\tan\theta_1 \tan\theta_3 + K_2 \tan\theta_1 \tan\theta_2 + K_1 \tan\theta_2 \tan\theta_3 - K_1 K_2 = 0 \quad (3)$$

Under CM excitation, the input impedance of Common Mode operation is given in (2). Therefore, by considering the denominator as equal to zero, the resonance frequencies of this mode could be calculated as:

$$\tan\theta_3 + K_2 \tan\theta_2 + K_1 K_2 \tan\theta_1 - K_1 \tan\theta_1 \tan\theta_2 \tan\theta_3 = 0 \quad (4)$$

Using (3) and (4), It could be seen that many different answers with regard to the parameters are achievable, which shows that multiple DM and CM resonance frequencies could be produced with different electrical lengths and characteristic impedances of the steps.

If $\theta_1 \neq \theta_2 \neq \theta_3$, the equation (3) and (4) are not analytically solvable, so a numerical approximation should be applied.

The primary resonance frequency of the circuit is a function of total electrical length $\theta_T=2(\theta_1+\theta_2+\theta_3)$ of stepped impedance resonator, and the position of higher-order resonance frequencies are linked to the parameters that follow: θ_1, θ_2, θ_3, K_1 and K_2. Therefore, in contrast to the conventional SIRs, non-proportional resonators provide additional freedom in design.

Using (3) and (4), and selecting constant values for θ_2 and θ_3, it is possible to draw design diagrams of f_3/f_1 and f_2/f_1 with different K_1 and K_2 values. In the same way for specific K_1 and K_2, frequency ratios of f_3/f_1 and f_2/f_1 with different θ_2 and θ_3 are achievable.

To clarify this methodology, design diagrams for specific electrical lengths (θ_2, θ_3) and characteristic impedance ratios (K_1, K_2) are drawn. For example, in Fig. 3, the DM frequency ratios of f_3/f_1 and f_2/f_1 with different K_1 and K_2 are presented for the particular $\theta_2=13.43°$ and $\theta_3=39.63°$.

Likewise, as presented in Fig. 4, the DM frequency ratios of f_3/f_1 and f_2/f_1 are depicted with different θ_2 and θ_3 for the particular $K_1 = 0.29$ and $K_2 = 3.78$. Consequently, it is quite simple to design the DM resonance frequencies of a balanced tri-band filter using the specific electrical lengths (θ_2, θ_3) in Fig. 3, or the characteristic impedance ratios (K_1, K_2) in Fig. 4.

As specified above, by having more design parameters, the balanced Ring-SIR provides additional degrees of freedom for controlling and adjusting the DM resonance frequencies. As mentioned, an appropriate selection of K_1 and K_2, and θ_2 and θ_3 could be made to reach the preferred DM resonance frequency ratios for outstanding out-of-band operation and CM resonance frequencies away from DM frequencies, which further help in improving CM rejection. Fig. 5 summarizes the design procedure of the tri-band balanced BPF using Ring-SIR resonator structures. The design process consists of 4 steps: first is to determine the required filter specification, second is to predesign the SIR structure of the balanced resonator and extracting the electrical length of SIR sections using design graphs, next calculating θ_1, Z_1, Z_2 and Z_3, and in the fourth step, we check the F_1 frequency for conformity with the design goals and then F_2 and F_3.
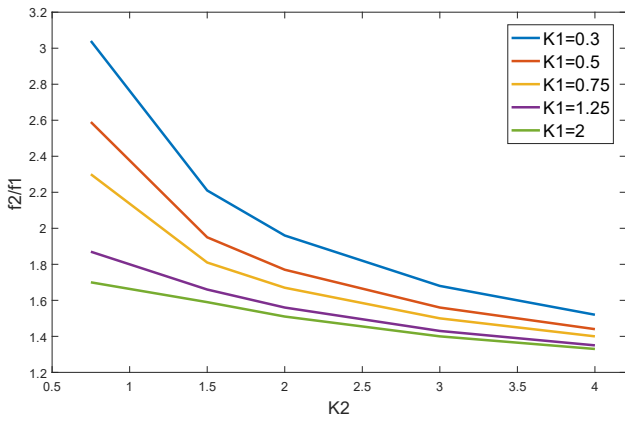
(a)
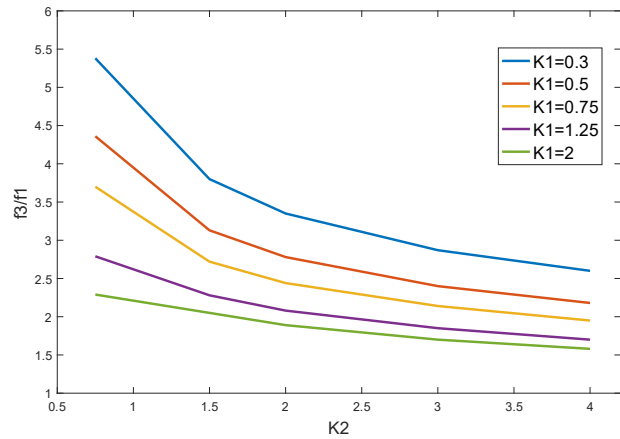
(b)

Fig. 3. The relation between DM frequency ratios of (a) f_2/f_1 and (b) f_3/f_1 for different K1 and K_2 values under the condition of θ_2=13.43° and θ_3=39.63°
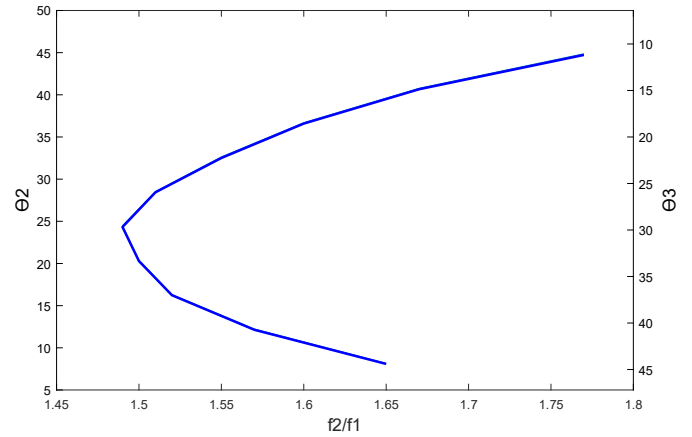
(a)
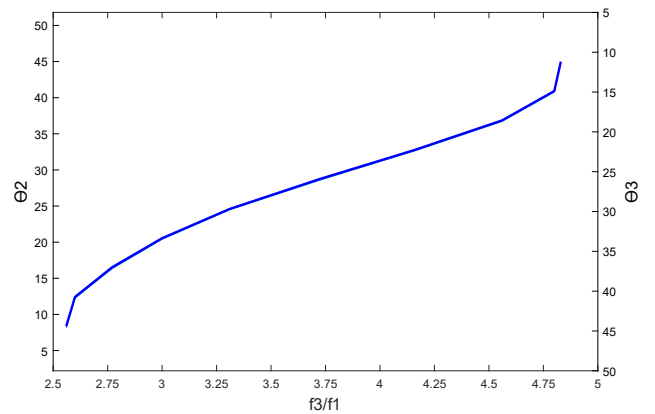
(b)

Fig. 4. Differential mode frequency ratios of (a) f_2/f_1 & (b) f_3/f_1 with different θ2 and θ3 under the condition of K_1=0.29 and K_2=3.78.
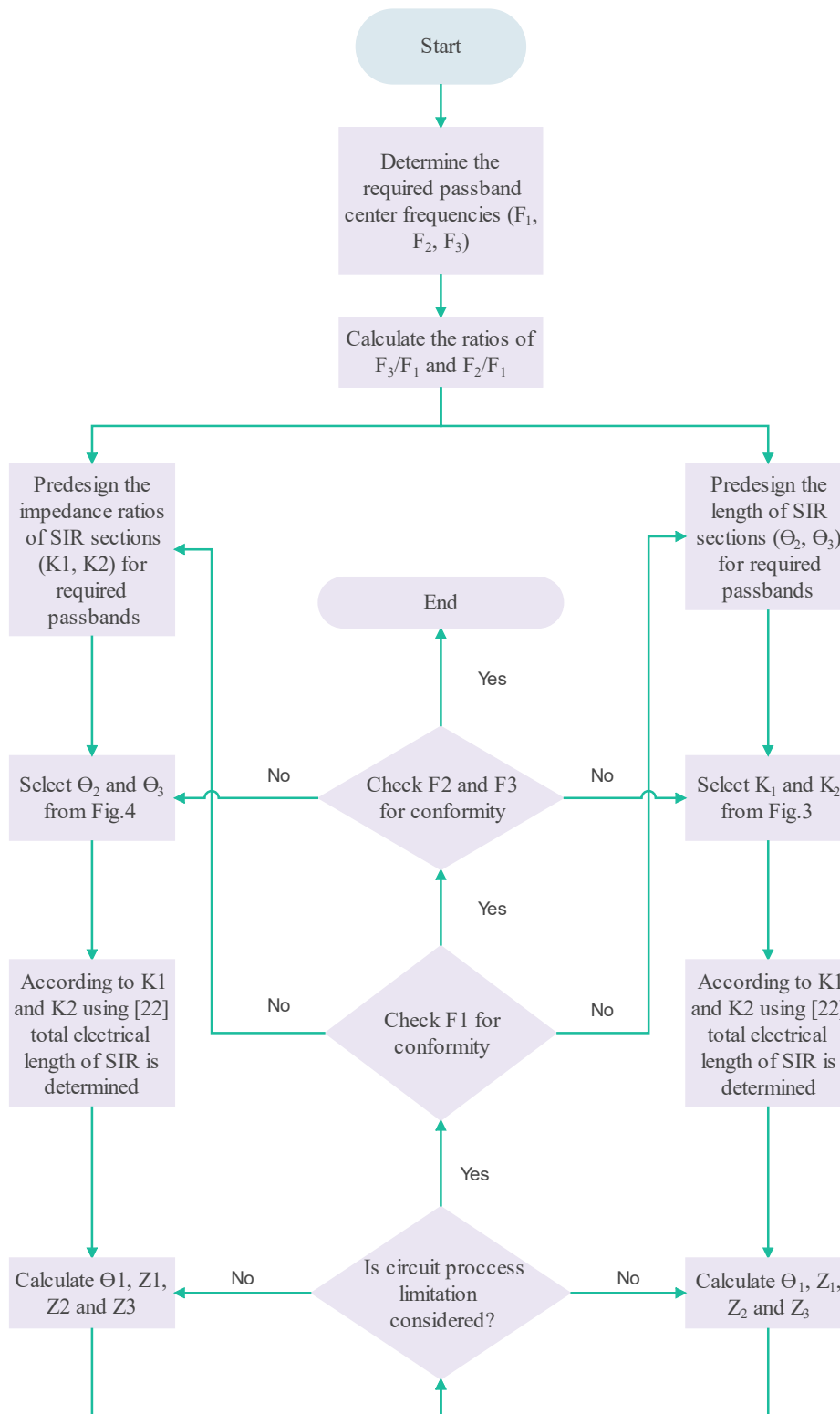
Fig. 5. Flowchart for obtaining the design parameters of the proposed balanced filter

3- Simulation of Balanced Networks

Simulation methods have a significant role in design and implementation of balanced BPFs, and several software suites are provided to perform the full EM simulation. In this section, differential and Common Mode simulation methods that can be carried out with Keysight Advanced Design System (ADS) software are described. However, different analytical software such as CST and HFSS can also be used.

3- 1- Single-ended Port DM and CM Simulations

Initially, the structure should be drawn using 50-Ω input/output (I/O) ports connected to all ports. Afterwards, the simulation is performed to obtain the matrix of 4x4 S-parameters for all frequencies. Differential-mode S-parameters can be determined by inserting the transformation equations given in (5) into the data display window.

$$S_{DD11} = 0.5(S_{11} - S_{21} - S_{12} + S_{22})$$
$$S_{DD12} = 0.5(S_{13} - S_{23} - S_{14} + S_{24})$$
$$S_{DD21} = 0.5(S_{13} - S_{41} - S_{32} + S_{42})$$
$$S_{DD22} = 0.5(S_{33} - S_{43} - S_{34} + S_{44})$$

$$S_{CD11} = 0.5(S_{11} + S_{21} - S_{12} - S_{22})$$
$$S_{CD12} = 0.5(S_{13} + S_{23} - S_{14} - S_{24})$$
$$S_{CD21} = 0.5(S_{13} + S_{41} - S_{32} - S_{42})$$
$$S_{CD22} = 0.5(S_{33} + S_{43} - S_{34} - S_{44})$$

$$(5)$$

$$S_{DC11} = 0.5(S_{11} - S_{21} + S_{12} - S_{22})$$
$$S_{DC12} = 0.5(S_{13} - S_{23} + S_{14} - S_{24})$$
$$S_{DC21} = 0.5(S_{13} - S_{41} + S_{32} - S_{42})$$
$$S_{DC22} = 0.5(S_{33} - S_{43} + S_{34} - S_{44})$$

$$S_{CC11} = 0.5(S_{11} + S_{21} + S_{12} + S_{22})$$
$$S_{CC12} = 0.5(S_{13} + S_{23} + S_{14} + S_{24})$$
$$S_{CC21} = 0.5(S_{13} + S_{41} + S_{32} + S_{42})$$
$$S_{CC22} = 0.5(S_{33} + S_{43} + S_{34} + S_{44})$$

3- 2- Differential Ports DM and CM Simulations

The circuit can be analyzed under differential-mode operation by replacing the single-end I/O ports with differential ones using port editor window. There are four pins; two of which are linked to the differential input port and the other two are linked to the differential output port. The impedances of I/O ports are adjusted to 100-Ω.

3- 3- Common Ports for CM Simulation

Replacing the single-end I/O ports with CM ports, the circuit can be analyzed under CM operation. There are four pins; two of which are linked to the common input port and the other two are linked to the common output port. Under this condition, each port must have a 25-Ω impedance.

4- Design of The Tri-band Balanced Filter
4- 1- Filter Design

For demonstration, a balanced tri-band band-pass filter with wide DM upper stop-band, exceptional performance and high CM rejection are designed. DM resonance frequencies of the desired tri-band balanced Band-pass SIR filter are centered at 1.7, 2.62, and 4.44 GHz. Thus, differential mode frequency ratios are computed to be: $f_2/f_1 = 2.62/1.70 \approx 1.54$ and $f_3/f_1 = 4.44/1.70 \approx 2.61$. With the specified $\theta_2 = 13.43°$ and $\theta_3 = 39.63°$ in Fig. 3(a), $K_1 = 0.29$ and $K_2 = 3.78$ are found, later, under the condition of $K_1 = 0.29$ and $K_2 = 3.78$. Consider the circuit process limitation, $Z_3 = 125.2\ \Omega$ is chosen. Afterwards, $Z_2 = 33$ and $Z_1 = 111.4\ \Omega$ are achieved. Based on $K_1 = 0.29$ and $K_2 = 3.78$, the total electronic length $\theta_T = 81.6°$ could be calculated [1]. The electrical length of the first section (θ_1) is then 28.54°.

In the same way, this process can be performed from Fig. 4 by specific values of K_1 and K_2. Two-order Butterworth tri-band balanced Band-pass filter with center frequencies of 1.7, 2.6, and 4.5 GHz and fractional bandwidths of 4%, 5% and 1.6% is designed and fabricated on the Rogers RO4003C substrate with a relative dielectric constant of 3.55, a thickness of 0.813mm and a loss tangent of 0.0022, which its configuration is shown in Fig. 6. Dual feed lines were employed to help control the external quality factors of three DM passbands. Hence, with different t values, the external quality factors can be controlled.
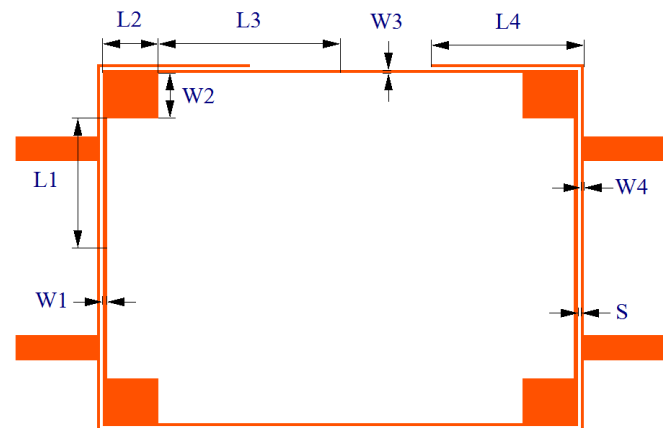
Fig. 6. Configuration of the proposed tri-band balanced BPF

Table 1. The geometrical parameters of the designed filter (mm).

Parameter	L1	L2	L3	L4	W1	W2	W3	W4	S
Value	8.95	3.85	12.55	10.5	0.3	3.1	0.2	0.2	0.2

Table 2. Second and Third band separation with different values of t (tap position)

t(mm)	1	2	3	4	5	6	7	8	9	10
Valley (dB)	36.21	30.61	27.12	24.5	22.15	19.89	17.63	15.2	12.72	10.56
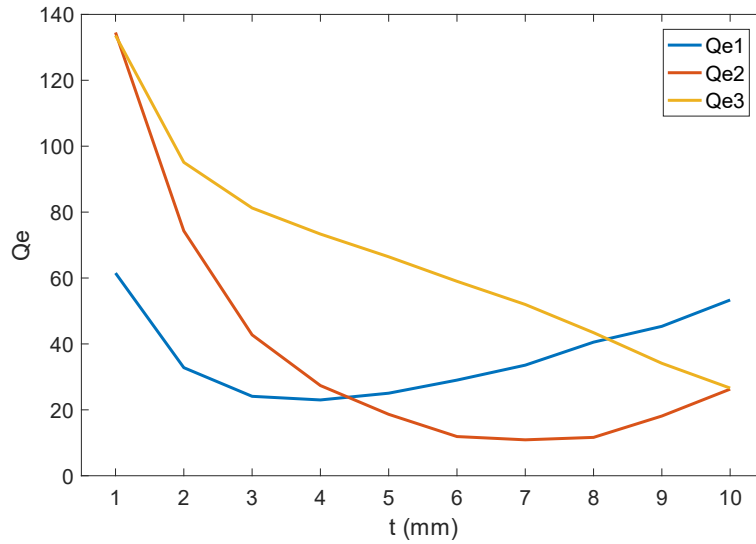
Fig. 7. External quality factor Qe for different feed line positions.

4- 2- External Quality Factor

Using filter specification, the input external quality factors for the first, second and third pass-bands are calculated with equation (7), where g_i are the element values of the low pass prototype filter response.

$$Q_{e1} = \frac{g_0 g_1}{FBW} \qquad Q_{en} = \frac{g_n g_{n+1}}{FBW} \qquad (7)$$

The external quality factors Qe can be extracted by full-wave electromagnetic simulation [2]. Qe varies with the width W4 of the feed lines, the length L4 of the feed lines, and the position parameter t. It can be observed from Fig. 7 that all the external quality factors of three pass-bands depend on t. Ultimately, the external quality factors for each pass-band are designed by adjusting the feeding position and coupling line length (L4=10.5mm) and width (W4=0.2mm). Fig. 7 demonstrates the relation of Qe1, Qe2 and Qe3 values with respect to feeding position, t. As shown in Fig. 7, t is the edge-to-edge distance from the feed line to the symmetry line of the circuit. The variation of Qe with respect to the t is plotted in Fig. 7. From this figure, the appropriate tap position leading to calculated external quality factors (Qe1=25, Qe2=20 and Qe3=62.5) is found to be 4.9mm. After a tuning process, the final value for tap position is set to t=4.5mm. Additionally, it has to be mentioned that as the circuit is symmetrical, the input and output external quality factors are the same. Another factor to consider in the quality factor analysis is the separation between the bands, which is an important parameter in multiband filters. Table 2 shows the values of the valley between the second and third bands with different t positions. Considering the design diagrams and Table 2, t is selected to be 4.50 mm to achieve the preferred Qe1, Qe2 and Qe3.

5- Analysis of Current Density Distribution

The current density distribution is introduced in this part to highlight the tri-band balanced operating characteristics of the BPF.

Fig. 8 depicts the surface current density distributions for DM and CM at frequencies of 1.7 GHz, 2.6 GHz, and 4.5 GHz (pass-band center frequencies), in addition to 2.26 GHz and 3.9 GHz (as a representative of DM valleys between pass-bands). The current between the I/O ports of the filter at f_1=1.7 GHz, f_2=2.55 GHz and f_3 = 4.48 GHz is evident in differential mode (Fig. 8(a, b, c)); however, the current between the I/O ports at 2.26 and 3.9 GHz (Fig. 8(g, h)) is non-existent. At 1.7, 2.55, and 4.48 GHz, under common-mode excitation, the current between the I/O ports does not exist. (Fig. 8(d, e, f))
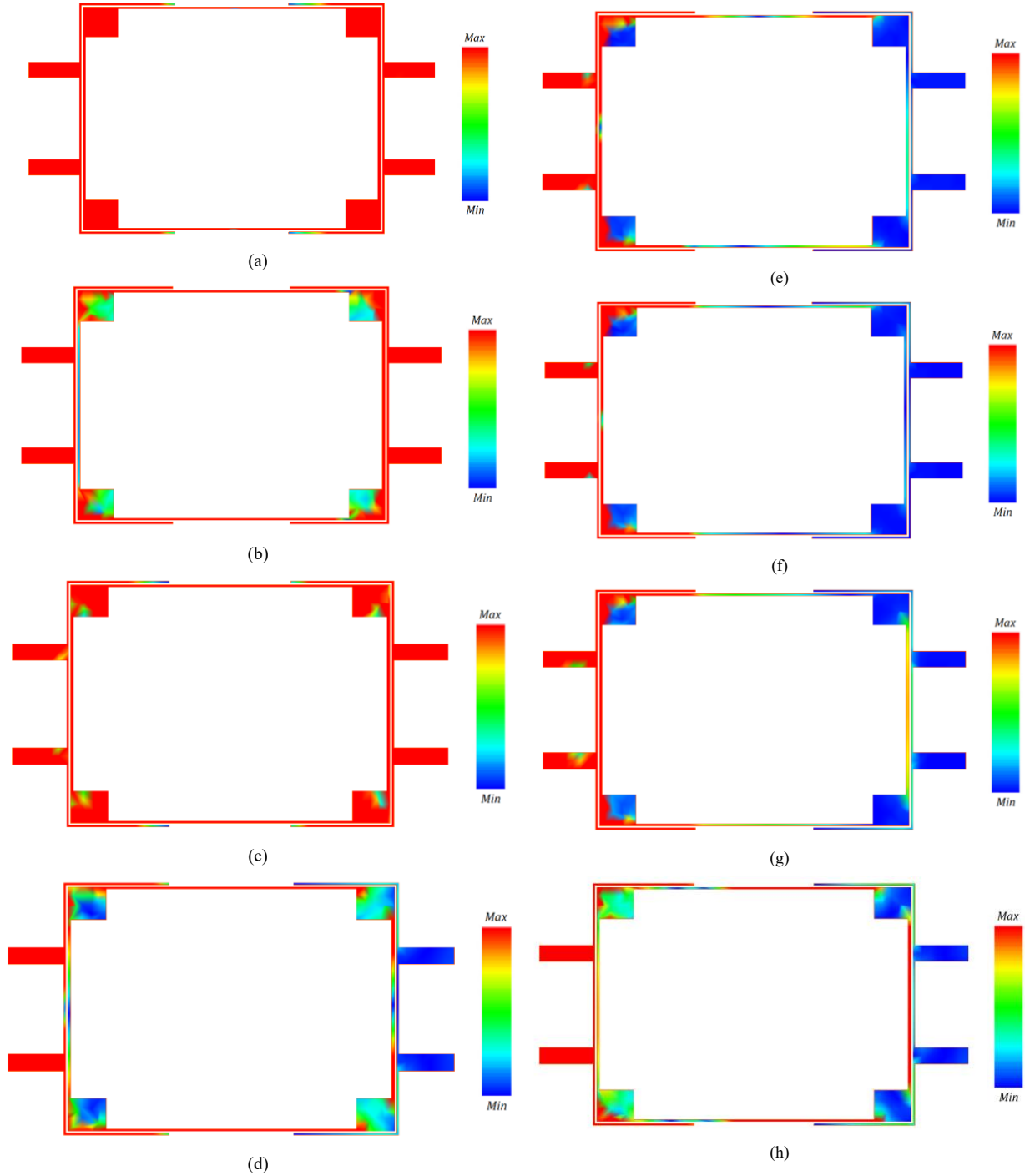
Fig. 8. The current distribution for the presented BPF in differential mode at pass-band center frequencies of (a) 1.7GHz, (b) 2.55GHz, (c) 4.48GHz, and the valleys in between at (g) 2.26GHz, (h) 3.9GHz and Common Mode at center frequencies of (d) 1.7GHz, (e) 2.55GHz, (f) 4.48GHz.

Table 3. Comparison of the presented balanced filter with its tri- band counterparts

Ref	Center Frequency (GHz)			Insertion Loss (dB)			Return Loss (dB)			3-db FBW (%)			CMS level (dB)			DM stopband	Effective Dimension (λg)	Manufacturing Technology
	f_1	f_2	F_3	IL_1	IL_2	IL_3	RL_1	RL_2	RL_3	Δ_1	Δ_2	Δ_3	1	2	3			
[18]	1.65	2.45	3.50	0.082	0.11	0.12	20	22	23	2.9	3.2	1.8	36	55	35	$3.03f_1$	0.34x0.26	HTS
[23]	2.45	3.5	4.45	1.44	1.68	2.16	13	8	20	17.9	5.7	15.7	>40	>40	>40	$2.45f_1$	0.68x0.29	DGS
[24]	2.76	5.7	7.63	0.9	1.7	2.2	17	8	15	13	5.7	3.7	-	-	-	$4.34f_1$	0.24x0.11	Via
[25]	2.44	3.6	5.5	1.6	2.2	0.5	12	14	18	4.8	2.2	25.3	-	-	-	$3.7f_1$	0.21x0.16	-
[26]	2.39	3.51	5.18	<1.7	<1.7	<1.7	34	26	29	11.6	4.2	6.7	-	-	-	$3.76f_1$	0.53x0.55	Lumped Elements, Via
[11]	0.85	1.57	2.4	0.98	1.1	0.96	~11	~12	~10.5	16.84	3.5	9.6	-	-	-	$3.3f_1$	0.10x0.09	Via
[27]	2.45	3.50	5.25	0.71	0.92	0.67	~20	~25	~20	1.22	2	1.52	38	32	25	$3.34f_1$	0.56x0.43	-
[12]	1.51	2.13	2.78	0.74	1.29	1.41	20.4	15.7	12.8	12	7.3	7	36.7	59	48	$2.38f_1$	0.74x0.75	Via
[28]	1.83	2.1	2.47	2.31	2.25	3.01	~27	~19.5	~17	3.01	2.86	2.31	-	-	-	$~2.5f_1$	0.22x0.22	Multi-layers, SIW, Via
This work	1.7	2.55	4.48	1.44	1.77	2.11	15.69	17.04	14.32	3.95	4.10	1.56	12.9	18.9	43.5	$5.15f_1$	0.31x0.23	-

Figure 8 shows that in the first band (1.7 GHz), the current is passed between the I/O ports by practically all parts of the resonator. For the second band at 2.55 GHz, current density at the corner of rectangular patches are weak. The third band current density at 4.48 GHz shows relatively low density at the joint of rectangular patches and 0.3 mm TLs.

Under common-mode excitation at pass-bands, it is evident that the symmetric design of the filter suppresses the signal in the parts near the input ports of the filter.

6- Results and Discussion

The measurement results of the filter shown in Fig. 6 under DM and CM excitations are depicted in Fig. 10. The filter has three pass-bands with center frequencies of 1.7, 2.55, and 4.48 GHz. The measurement results meet the desired DM specs with reasonably low IL (1.44 dB measured at f_1^d, 1.77 dB measured at f_2^d and 2.11 dB measured at f_3^d). Return losses for each pass-band are better than 15.69, 17.04, and 14.32 dB, respectively. The 3dB fractional bandwidth are 3.95%, 4.10% and 1.56% separately. Good common-mode suppression is found for this filter, especially for the third pass-band as clearly implied by the S_{21CC} measurement result (around 12.9dB for first, 18.9 for second, and 43.5dB for third pass-band).

Furthermore, the differential-mode operation has been exceptionally well in the out of band region, since the insertion loss is below 20 dB until 8.76 GHz and no spurious pass-bands are observed. Another factor to consider is the separation between the bands, which is an essential parameter in multiband filters. In this filter, the value of pass-band separation between the first two bands is 62.04dB, and is 15.46dB between the second and third bands. The filter selectivity has excellent performance, and the filter has steep skirts. Besides its outstanding performance, this filter was designed

utilizing a well-known standard design approach with no concern about CM rejection. The CM resonance frequencies are distant from DM resonances resulting in good CM suppression in pass-bands of the filter.

The total size of the circuit is 33.6mm x 25.3mm, equal to $0.31\lambda_g$ x $0.23\lambda_g$, in which λ_g denotes the microstrip line guided wavelength at the center frequency of the first band. Table 3 compares some of the characteristics of tri-band balanced and unbalanced BPFs presented in the recent years. In this table, f_1, f_2 and f_3 are the center frequencies of the first, second, and third pass-bands, respectively. Additionally, at the first, second, and third bands, IL_1, IL_2 and IL_3 are the insertion losses, and RL_1, RL_2 and RL_3 are the return losses, respectively. Δ_1, Δ_2 and Δ_3 represent the 3dB fractional bandwidths. CMS level shows the in-band value of S_{21CC} for each pass-band. This table also compares the stop-band bandwidth of the dual band balanced BPFs in terms of the ratio of their first center frequency.

Table 3 shows that the proposed filter has parameters better than or on parallel with the other filters mentioned, with the advantage of a simple manufacturing technology without Via, DGS, Multilayer fabrication, lumped elements, and HTS materials which result in cheaper and more accurate fabrication.

The stopband bandwidth, which was an essential factor in the design process of the presented filter, is an additional benefit for BPFs in general. In comparison to other references, the presented balanced filter has the highest stop-band bandwidth, as shown in the table. The measured insertion loss shows relatively low-loss in all three pass-bands. Additionally, in balanced filters, the CM response has significant importance and the proposed filter has the highest CM suppression for the third band among the quoted references except for [12], while the first and second pass-bands have

(a)   (b)
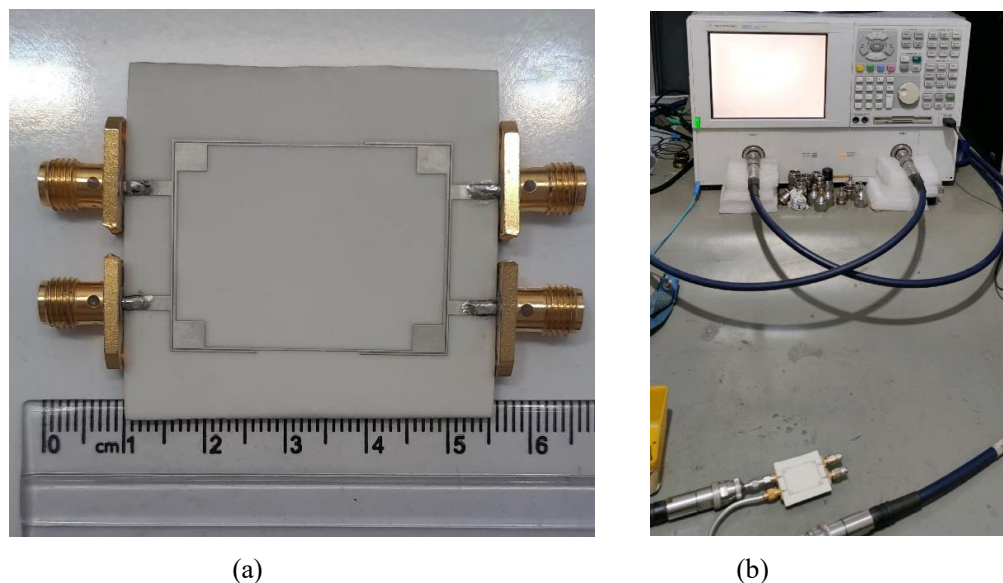
Fig. 9. (a) Fabricated prototype of the proposed filter. (b) One of measurement setups with VNA
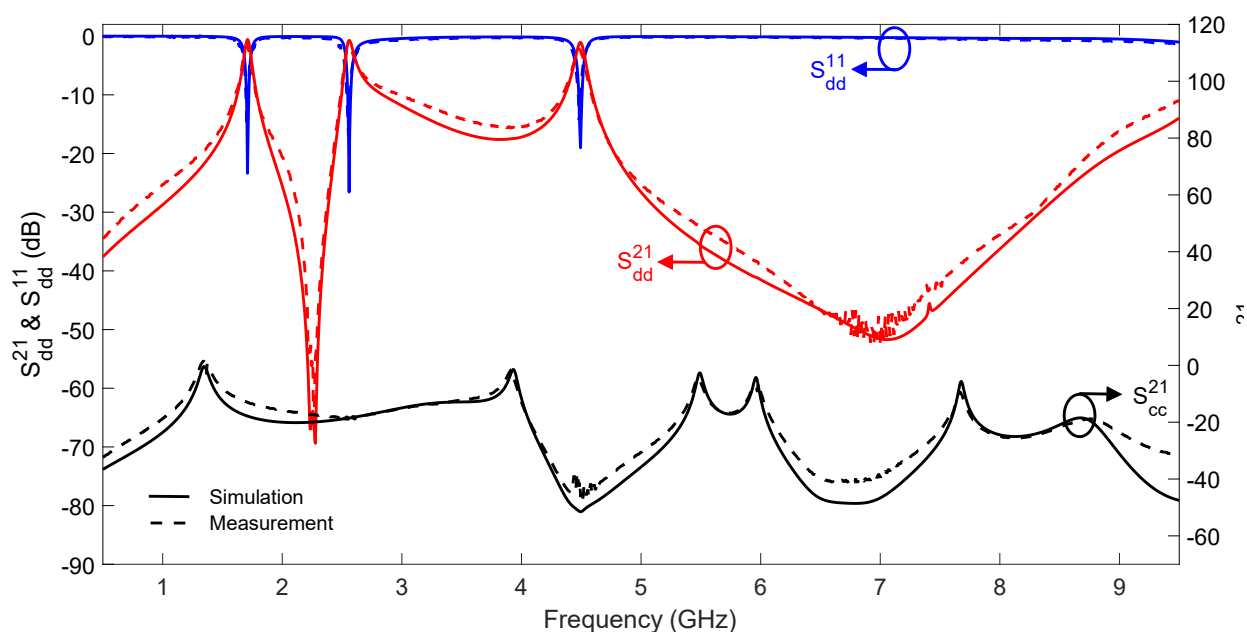
Fig. 10. Simulated and Measured S-parameters of the tri-band balanced filter.

satisfactory common-mode suppression. It is worth noting that there is always a trade-off among filter design parameters. Thus, apart from [3] which has used the unpractical HTS technology, in addition to a large upper stopband bandwidth, the presented tri-band balanced bandpass filter also has other desirable characteristics, including good return loss and CM suppression.

Finally, one of the most distinguishing characteristics of a balanced BPF is its dimensions, and table 3 compares the size of the presented filter against its counterparts in terms of λ_g. It is evident that compared to balanced filters of [4], [5], [6] and [7], the presented configuration is the most compact tri-band balanced filter without using complicated manufacturing structures among the mentioned topologies.

7- Conclusion

A novel planar microstrip tri-band balanced BPF based on the Ring-SIR structure has been presented. The suggested configuration provides additional benefits in controlling the DM and CM resonance frequencies, as shown in the results, the pass-bands of the presented filter can be adjusted by tuning a specified aspect length. The current density distribution of the filter is provided. The outstanding features of the presented balanced BPF are its minimal dimensions, ultra-wide upper DM stopband bandwidth, reconfigurable frequencies, CM suppression, sharp skirt response, and high suppression in stopbands. Considering these excellent specifications, it could be useful for Advanced Wireless Services (AWS), LTE, and long-distance radio telecommunication applications.

The proposed filter is designed and analyzed. Measurements are made using Agilent E8362B PNA network analyzer. This filter is fabricated on a Rogers substrate with small dimensions of 33.6mm x 25.3mm or 0.31 λ_g × 0.23 λ_g, λ_g is the wavelength at the central frequency of the first pass-band.

References

[1] R. Levy and S. Cohn, "A history of microwave filter research, design, and development," IEEE Trans. Microw. Theory Tech, vol. 32, no. 9, pp. 1055-1067, 1984.

[2] J. S. Hong and M. J. Lancaster, Microstrip filters for rf/microwave applications, NY: Wiley, 2001.

[3] Y. Kuo and C. Chang, "Analytical design of two-mode dual-band filters using E-shaped resonators," IEEE Transactions on Microwave Theory and Techniques, vol. 60, no. 2, pp. 250-260, 2012.

[4] Z. Chunxia, G. Yongxin and Y. Shaolin, "A compact dual-band filter based on dual-mode resonators," in Proceedings of Asia-Pacific Microwave Conference, 2011.

[5] Y. Liu, Y. Zhao, Y. Zhou and Z. Niu, "Integrated dual-band BPF and single-band BSF for tri-band filter design," Journal of Electromagnetic Waves and Applications, vol. 25, no. 17, pp. 2420-2428, 2011.

[6] S. Fu, B. Wu, J. Chen, S. Sun and C. Liang, "Novel second-order dual-mode dual-band filters using capacitance loaded square loop resonator," IEEE Transactions on Microwave Theory and Techniques, vol. 60, no. 3, pp. 477-483, 2011.

[7] B. Ren, H. Liu, Z. Ma, M. Ohira, P. Wen, X. Wang and a. X. Guan, "Compact dual-band differential bandpass filter using quadruple-mode stepped-impedance square ring loaded resonators," IEEE Access, vol. 6, p. 21850–21858, 2018.

[8] Y. Chang, C. Kao, M. Weng and R. Yang, "Design of the compact dual-band bandpass filter with high isolation for GPS/WLAN applications," IEEE Microwave and Wireless Components Letters, vol. 19, no. 12, pp. 780-782, 2009.

[9] M. Doan, W. Che and W. Feng, "Tri-band bandpass filter using square ring short stub loaded resonators," IET Electronics Letters, vol. 48, no. 2, pp. 106-107, 2012.

[10] W. Chen, M. Weng and S. Chang, "A new tri-band bandpass filter based on stub-loaded step-impedance resonator," IEEE Microwave and Wireless Components Letters, vol. 22, no. 4, pp. 179-181, 2012.

[11] A. Basit, M. I. Khattak, A. R. Sebak, A. B. Qazi and A. A. Telba, "Design of a Compact Microstrip Triple Independently Controlled Pass Bands Filter for GSM, GPS and WiFi Applications," IEEE Access, vol. 8, pp. 77156-77163, 2020.

[12] R. Gómez-García and R. Loeches-Sánchez, "Multi-Stub-Loaded Differential-Mode Planar Multiband Bandpass Filters," IEEE Transactions on Circuits and Systems II: Express Briefs, vol. 65, no. 3, pp. 271-275, 2018.

[13] F. Wei, Y. J. Guo, P.-Y. Qin and X. W. Shi, "Compact Balanced Dual- and Tri-band Bandpass Filters Based on Stub Loaded Resonators," IEEE Microwave and Wireless Components Letters, vol. 25, no. 2, pp. 76-78, 2015.

[14] H. Liu, Z. Wang, S. Hu, H.-X. Xu and B. Ren, "Design of Tri-Band Balanced Filter with Wideband Common-Mode Suppression and Upper Stopband Using Square Ring Loaded Resonator," IEEE Transactions on Circuits and Systems II: Express Briefs, vol. 67, no. 10, pp. 1760-1764, 2019.

[15] S.-X. Zhang, L.-L. Qiu and Q.-X. Chu, "Multiband Balanced Filters With Controllable Bandwidths Based on Slotline Coupling Feed," IEEE Microwave and Wireless Components Letters, vol. 27, no. 11, pp. 974-976, 2017.

[16] H. Liu, Y. Song, B. Ren, P. Wen, X. Guan and H. Xu, "Balanced Tri-Band Bandpass Filter Design Using Octo-Section Stepped-Impedance Ring Resonator with Open Stubs,"IEEE Microwave and Wireless Components Letters, vol. 27, pp. 912-914, 2017.

[17] F. Wei, C.-Y. Zhang, H.-J. Yue and X.-W. Shi, "Balanced Quad-Band Bandpass Filter With Controllable Frequencies and Bandwidths," IEEE Access, vol. 7, pp. 140470 - 140477, 2019.

[18] J. Zhang, Q. Liu, H. Liu, D. Zhang and D. Zhou, "Compact balanced tri-band superconducting band-pass filter using double square ring loaded resonators," Int J RF Microw Comput Aided Eng, vol. 31, no. 3, 2021.

[19] Y. Al-Yasir, N. Ojaroudi Parchin, A. Abdulkhaleq, M. Bakr and Abd-Alhameed, "A Survey of Differential-Fed Microstrip Bandpass Filters: Recent Techniques and Challenges," Sensors, vol. 20, no. 2356, 2020.

[20] V. CRNOJEVIC´-BENGIN, Advances in Multi-Band Microstrip Filters, Cambridge: Cambridge University Press, 2015.

[21] F. Martín, L. Zhu, J. Hong and F. Medina, Balanced Microwave Filters, Hoboken, NJ: John Wiley & Sons, Inc., 2018.

[22] D. Packiaraj, M. Ramesh and A. T. Kalghatgi, "Design of a tri-section folded SIR filter," IEEE Microw. Wireless Compon. Lett., vol. 16, no. 5, pp. 317-319, 2006.

[23] Y. Yang, Z. Wang, L. Xu and Y. Liu, "A balanced tri-band bandpass filter with high selectivity and controllable bandwidths," Int J RF Microw Comput Aided Eng, vol. 29, no. 12, 2019.

[24] C. Wang, X. Xi, Y. Zhao and X. Shi, "A miniaturized tri-band bandpass microstrip filter using multiple resonators

with sharp skirts," International Journal of Microwave and Wireless Technologies, vol. 13, no. 5, pp. 430-434, 2021.

[25] I. Jadidi, M. A. Honarvar and F. Khajeh-Khalil, "Compact Tri-Band Microstrip Filter Using Three Types of Resonators for Bluetooth, WiMAX , and WLAN Applications," Progress In Electromagnetics Research C, vol. 91, pp. 241-252, 2019.

[26] A. Bandyopadhyay, P. Sarkar, T. Mondal and R. Ghatak, "A Dual Function Reconfigurable Bandpass Filter for Wideband and Tri-Band Operations," IEEE Transactions on Circuits and Systems II: Express Briefs, vol. 68, no. 6, pp. 1892-1896, 2021.

[27] H. Liu, Z. Wang, S. Hu, H. -X. Xu and B. Ren, "Design of Tri-Band Balanced Filter With Wideband Common-Mode Suppression and Upper Stopband Using Square Ring Loaded Resonator," IEEE Transactions on Circuits and Systems II: Express Briefs, vol. 67, no. 10, pp. 1760-1764, 2020.

[28] M. Ho and K. Tang, "Miniaturized SIW Cavity Tri-Band Filter Design," IEEE Microwave and Wireless Components Letters, vol. 30, no. 6, pp. 589-592, 2020.

[29] L. Xu, H. Yue, F. Wei and X. Shi, "A balanced dual-band bandpass filter with a wide stopband and controllable differential-mode frequencies and fractional bandwidths," International Journal of RF and Microwave Computer-Aided Engineering, 2020.

[30] M. Zhao, L. Xu, X. Cheng, W. Chen, W. Wu and F. Wei, "Design of a balanced dual-band BPF with high selectivity," Microw Opt Technol Lett, vol. 62, p. 3536–3541, 2020.

[31] F. Bagci, A. Fernández-Prieto, A. Lujambio, J. Martel, J. Bernal and F. Medina, "Compact Balanced Dual-Band Bandpass Filter Based on Modified Coupled-Embedded Resonators," IEEE Microwave and Wireless Components Letters, vol. 27, no. 1, pp. 31-33, 2017.

[32] G. Dong, W. Wang, Y. Wu, W. Li, Y. Liu and M. M. Tentzeris, "Dual-Band Balanced Bandpass Filter Using Slotlines Loaded Patch Resonators With Independently Controllable Bandwidths," IEEE Microwave and Wireless Components Letters, vol. 30, no. 7, pp. 653-656, 2020.

[33] G. Karimi, M. Amirian, A. Lalbakhsh and M. Ranjbar, "A new microstrip coupling system for realization of a differential dual-band bandpass filter," AEU - International Journal of Electronics and Communications, vol. 99, pp. 186-192, 2019.

[34] Q. Zhang, C. Chen, W. Chen, D. J. and H. Zhang, "Novel balanced single/dual-band bandpass filters based on a circular patch resonator," IET Microw. Antennas Propag, vol. 15, pp. 206-220, 2021.